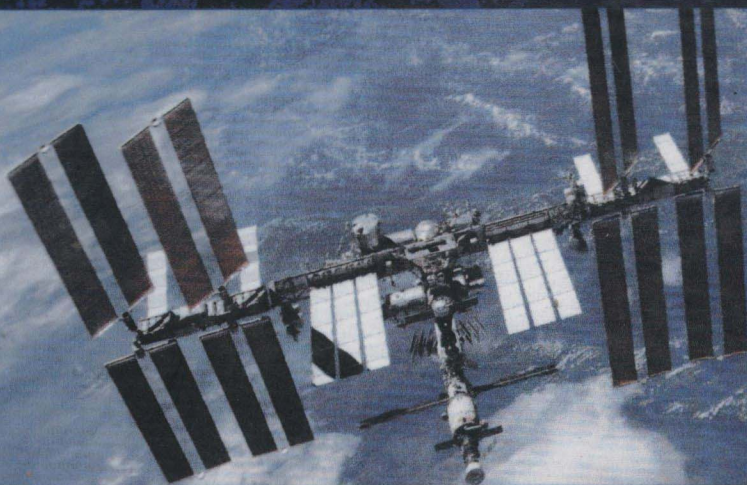


7TH
EDITION

THE FINITE ELEMENT METHOD
FOR SOLID & STRUCTURAL
MECHANICS

有限元方法：固体力学和结构力学 第7版



O.C. Zienkiewicz, R.L. Taylor and D.D. Fox

Elsevier (Singapore) Pte Ltd.

世界图书出版公司
www.wpcbj.com.cn

The Finite Element Method for Solid and Structural Mechanics

Seventh Edition

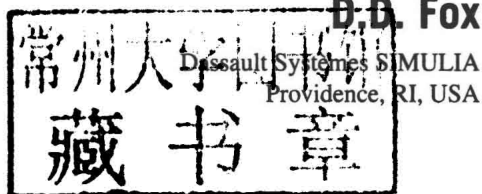
O.C. Zienkiewicz, CBE, FRS

Previously UNESCO Professor of Numerical Methods in Engineering
International Centre for Numerical Methods in Engineering, Barcelona, Spain
Previously Director of the Institute for Numerical Methods in Engineering
University of Wales Swansea, UK

R.L. Taylor

Professor in the Graduate School
Department of Civil and Environmental Engineering
University of California at Berkeley
Berkeley, CA, USA

D.D. Fox



AMSTERDAM • BOSTON • HEIDELBERG • LONDON
NEW YORK • OXFORD • PARIS • SAN DIEGO
SAN FRANCISCO • SINGAPORE • SYDNEY • TOKYO

Butterworth-Heinemann is an imprint of Elsevier



The Finite Element Method for Solid and Structural Mechanics

Professor O.C. Zienkiewicz, CBE, FRS, FREng died on January 2, 2009. Prior to his death he was Professor Emeritus at the Civil and Computational Engineering Centre, University of Wales, Swansea and previously was Director of the Institute for Numerical Methods in Engineering at the University of Wales, Swansea, UK. He also held the UNESCO Chair of Numerical Methods in Engineering at the Technical University of Catalunya, Barcelona, Spain. He was the head of the Civil Engineering Department at the University of Wales, Swansea between 1961 and 1989. During this period he established that department as one of the primary centers of finite element research. In 1968 he became the Founder Editor of the *International Journal for Numerical Methods in Engineering* which still remains today the major journal in this field. The recipient of 27 honorary degrees and many medals, Professor Zienkiewicz was a member of five academies—an honor he received for his many contributions to the fundamental developments of the finite element method. In 1978, he became a Fellow of the Royal Society and the Royal Academy of Engineering. This was followed by his election as a foreign member to the US Academy of Engineering (1981), the Polish Academy of Science (1985), the Chinese Academy of Sciences (1998), and the National Academy of Science, Italy (Accademia dei Lincei) (1999). He published the first edition of this book in 1967.

Professor R.L. Taylor has more than 50 years' experience in the modeling and simulation of structures and solid continua including 8 years in industry. He is Professor of the Graduate School and the Emeritus T.Y. and Margaret Lin Professor of Engineering at the University of California at Berkeley and also Corporate Fellow at Dassault Systèmes SIMULIA in Providence, Rhode Island. In 1991 he was elected to membership in the US National Academy of Engineering in recognition of his educational and research contributions to the field of computational mechanics. Professor Taylor is a Fellow of the US Association of Computational Mechanics—USACM (1996) and a Fellow of the International Association of Computational Mechanics—IACM (1998). He has received numerous awards including the Berkeley Citation, the highest honor awarded by the University of California at Berkeley, the USACM John von Neumann Medal, the IACM Gauss-Newton Congress Medal, and a Dr.-Ingenieur Ehrenhalber awarded by the Technical University of Hannover, Germany.

Dr. D.D. Fox has more than 26 years' experience in the research and development of finite element technology. During the last 22 years he has worked at Dassault Systèmes SIMULIA, makers of the Abaqus finite element software program; where he has held various positions ranging from finite element software developer to development group manager. Currently, he is Senior Director in SIMULIA's CTO Office responsible for research into innovative uses of simulation technology in science and engineering. Dr. Fox was awarded his doctoral degree in 1990 from the Division of Applied Mechanics at Stanford University, working under the supervision of Professor Juan Carlos Simo. Dr. Fox is the author of many technical papers on finite element methods, including a seminal series on a stress resultant geometrically exact shell model that resulted in seven parts, covering the mathematical theory, linear and nonlinear finite element implementation, thickness change effects, nonlinear constitutive behavior, transient dynamics simulation, and shell intersections. This highly cited series helped usher in the modern mathematical approach to computational structural mechanics.

*This book is dedicated to Olgierd Cecil Zienkiewicz
and Juan Carlos Simo*

List of Figures

1.1	Finite element mesh for tire analysis: (a) tire cross-section; (b) full mesh.	2
1.2	Temperature contours on a disc brake system (provided by Livermore Software Technology Corporation).	2
1.3	Low-pressure die casting simulation. Temperature map in casting wheel and die components. Image courtesy of ESI Group and CMS.	3
1.4	Problem classes range from toys to full-scale systems. Images courtesy of Dassault Systèmes SIMULIA: (a) radio control toy race car; (b) Beechcraft aircraft.	4
1.5	Domain (Ω) and boundary parts for traction (Γ_U) and displacement (Γ_D).	8
2.1	Isoparametric map for four-node two-dimensional quadrilateral: (a) element in ξ coordinates and (b) element in x coordinates.	24
2.2	Boundary conditions for specified displacements.	35
2.3	Boundary conditions for specified traction.	37
2.4	Normal to surface.	38
2.5	Six-node triangular element for \mathbf{u} with linear p : (a) displacement nodes and (b) pressure nodes.	46
2.6	Estimation of thermophysical properties in phase change problems. The latent heat effect is approximated by a large capacity over a small temperature interval $2\Delta T$.	49
2.7	(a) Mesh; (b) Time dependent freezing zones.	49
2.8	Reactive sphere. Transient temperature behavior for ignition ($\bar{\delta} = 16$) and nonignition ($\bar{\delta} = 2$) cases: (a) induction time versus Frank–Kamenetskii parameter and temperature profiles; (b) temperature profiles for ignition ($\bar{\delta} = 16$) and nonignition ($\bar{\delta} = 2$) transient behavior of a reactive sphere.	50
2.9	Crash analysis: (a) mesh at $t = 0$ ms; (b) mesh at $t = 20$ ms; (c) mesh at $t = 40$ ms.	52
2.10	Retaining wall subjected to earthquake excitation: comparison of experiment (centrifuge) and calculations [28].	53
3.1	Possibility of multiple solutions.	58
3.2	Newton's method.	60

xviii List of Figures

3.3	The modified Newton method: (a) with initial tangent in increment; (b) with initial problem tangent.	62
3.4	The secant method starting from a K^0 prediction.	63
3.5	Direct (or Picard) iteration.	65
3.6	<i>Regula falsi</i> applied to line search: (a) extrapolation; (b) interpolation.	66
3.7	One-dimensional interpretation of the Bergan procedure.	69
3.8	Direct integration procedure.	71
4.1	Spring-dashpot models for linear viscoelasticity: (a) Maxwell element; (b) Kelvin element.	78
4.2	Typical viscoelastic relaxation function.	83
4.3	Standard linear viscoelastic solid: (a) model for standard solid; (b) relaxation function.	84
4.4	Mesh and loads for internal pressure on a thick-walled cylinder: (a) four-node quadrilaterals; (b) nine-node quadrilaterals.	87
4.5	Radial stress for internal pressure on a thick-walled cylinder: (a) mixed model; (b) displacement model.	88
4.6	Uniaxial behavior of materials: (a) nonlinear elastic and plastic behavior; (b) ideal plasticity; (c) strain hardening plasticity.	89
4.7	Yield surface and normality criterion in two-dimensional stress space.	90
4.8	Isotropic yield surfaces in principal stress space: (a) Drucker-Prager and Huber-von Mises; (b) Mohr-Coulomb and Tresca.	103
4.9	Loading and unloading directions in stress space.	108
4.10	A generalized plasticity model describing a very complex path, and comparison with experimental data. Undrained two-way cyclic loading of Nigata sand [68]. (Note that in an undrained soil test the fluid restrains all volumetric strains, and pore pressures develop; see Ref. [69].)	110
4.11	Perforated plane stress tension strip: mesh used and development of plastic zones at loads of 0.55, 0.66, 0.75, 0.84, 0.92, 0.98, and 1.02 times σ_y : (a) T3 triangles; (b) plastic zone spread; (c) Q4 quadrilaterals; (d) Q9 quadrilaterals.	112
4.12	Perforated plane stress tension strip: load deformation for strain hardening case ($H = 225 \text{ kg/mm}^2$).	113
4.13	Limit load behavior for plane strain perforated strip: (a) displacement (displ.) formulation results; (b) mixed formulation results.	114
4.14	Steel pressure vessel: (a) element subdivision and spread of plastic zones; (b) vertical deflection at point A with increasing pressure.	116
4.15	(a) Elasto-plastic; (b) elasto-viscoplastic; (c) series of elasto-viscoplastic models.	119

4.16	Creep in a pressure vessel: (a) mesh end effective stress contours at start of pressurization; (b) effective stress contours 3 h after pressurization.	122
4.17	Uniaxial, axisymmetric compression between rough plates: (a) mesh and problem; (b) pressure displacement result; (c) plastic flow velocity patterns.	123
4.18	Embankment under action of gravity, relative plastic flow velocities at collapse, and effective shear strain rate contours at collapse: (a) associative behavior; (b) nonassociative (zero volume change) behavior.	124
4.19	Underground power station: gravity and prestressing loads. (a) Elastic stresses; (b) "no-tension" stresses.	125
4.20	Cracking of a reinforced concrete beam (maximum tensile strength 200 lb/in ²). Distribution of stresses at various sections [106]: (a) mesh used; (b) section AA; (c) section BB; (d) section CC.	126
4.21	"Laminar" material: (a) general laminarity; (b) laminar in narrow joint.	128
4.22	Π plane section of Mohr-Coulomb yield surface in principal stress space, with $\phi = 25$ deg (solid line); smooth approximation of Eq. (4.175) (dotted line).	130
4.23	Nonuniqueness: mesh size dependence in extension of a homogeneous bar with a strain softening material. (Peak value of yield stress, σ_y , perturbed in a single element.) (a) Stress σ versus strain ε for material; (b) stress $\bar{\sigma}$ versus average strain $\bar{\varepsilon}(= u/L)$ assuming yielding in a single element of length h .	131
4.24	Illustration of a nonlocal approach (work dissipation in failure is assumed to be constant for all elements): (a) an element in which localization is considered; (b) localization; (c) stress-strain curve showing work dissipated in failure.	133
4.25	A nonlinear heat-generation problem illustrating the possibility of multiple or no solutions depending on the heat-generation parameter $\bar{\delta}$; spontaneous combustion [150]: (a) solution mesh and variation of temperature at point C; (b) two possible temperature distributions for $\bar{\delta} = 0.75$.	135
5.1	Reference and deformed (current) configuration for finite deformation problems.	148
6.1	Volumetric deformation.	183
6.2	Uniaxial stretch. Saint-Venant-Kirchhoff and neo-Hookean material. (M) denotes a modified compressible material.	186
6.3	Uniaxial stretch. Arruda-Boyce model.	188
6.4	Incremental deformation motions and configurations.	196
6.5	Necking of a cylindrical bar: eight-node elements. (a) Finite element model; (b) half-bar by symmetry.	201

xx List of Figures

6.6	Deformed configuration and contours for necking of bar. (a) First invariant (J_1); (b) second invariant (J_2).	202
6.7	Neck radius versus elongation displacement for a half-bar.	203
6.8	Adaptive refinement applied to the problem of a perforated strip. (a) The geometry of the strip and a very fine mesh are used to obtain an “exact” solution; (b) various stages of refinement aiming to achieve a 5% relative energy norm, error at each load increment (quadratic elements T6/3B/3D were used); (c) local displacement results.	204
6.9	Elongation of elements used to model the nearly one-dimensional behavior and the discontinuity.	206
6.10	Adaptive analysis of plastic flow deformation in a perforated plate. (a) Initial mesh, 273 degrees of freedom; (b) final adapted mesh; (c) displacement of an initially uniform grid embedded in the material.	207
6.11	Failure of a rigid footing on a vertical cut. Ideal von Mises plasticity and quadratic triangles with linear variation for pressure (T6/3C) elements are assumed. (a) Geometrical data; (b) coarse mesh; (c) final adapted mesh; (d) displacements after failure; (e) displacement-load diagrams for adaptive mesh and ideal plasticity ($H = 0$); (f) softening behavior. Coarse mesh and adapted mesh results are with a constant H of -5000 and a variable H starting from -5000 at coarse mesh size.	208
6.12	A $p - \delta$ diagram of elasto-plastic slope aiming at 2.5% error in ultimate load (15% incremental energy error) with use of quadratic triangular elements (T6/3B). Mesh A: $u = 0.0$ (coarse mesh). Mesh B: $u = 0.025$. Mesh C: $u = 0.15$. Mesh D: $u = 0.3$. Mesh E: $u = 0.45$. Mesh F: $u = 0.6$. Mesh G: $u = 0.75$. Mesh H: $u = 0.9$. The last mesh (mesh H, named the “optimal mesh”) is used for the solution of the problem from the first load step, without further refinement.	209
6.13	Foundation (eccentric loading); ideal von Mises plasticity. (a) Geometry and boundary conditions; (b) adaptive mesh; (c) deformed mesh using T6/1D elements ($H = 0, \nu = 0.49$).	210
6.14	Iceberg gouging of sea floor near buried oil pipelines. Image courtesy of Dassault Systemes SIMULIA and JP Kenny.	211
7.1	A 2D representative volume element mesh: (a) two material region; (b) RVE—mesh and nodes.	217
7.2	Periodic conditions on 2D RVE: (a) square RVE; (b) hexagonal RVE.	222
7.3	RVE for single fiber composite: (a) full RVE mesh; (b) cutaway showing fiber.	226
7.4	RVE for laminated plate.	228
7.5	RVE deformed shapes for fixed and periodic boundary conditions: (a) fixed displacement boundary; (b) periodic boundary.	228

7.6	Cylindrical bending of plate: (a) large displacement shape at maximum loading; (b) load displacement results for FE and FE^2 analyses.	229
7.7	Moment-curvature. Meshes for multiscale finite element solutions: (a) 12×12 unit cell mesh; (b) mesh for unit cell and RVE; (c) mesh for coarse scale.	230
7.8	Moment-curvature. Multiscale response vs. fine-scale finite element solution.	231
8.1	Contact between two bodies: (a) no contact condition; (b) contact state.	236
8.2	Contact by finite elements.	237
8.3	Contact between semicircular disks: node-node solution. (a) Undeformed mesh; (b) deformed mesh; (c) vertical stress contours.	238
8.4	Tied interface for a two region problem.	243
8.5	Node-to-surface contact: (a) contact using element interpolations; (b) contact using "smoothed" interpolations.	246
8.6	Node-to-surface contact: gap and normal definition.	247
8.7	Node-to-surface contact: normal vector description. (a) Normal to master facet; (b) normal to slave facet.	249
8.8	Increment of tangential slip.	259
8.9	Contact between semicircular disks: vertical contours for node-to-surface solution.	266
8.10	Contact between a disk and a block—frictionless solution: (a) initial mesh; (b) deformed mesh; (c) σ_1 stress; (d) σ_2 stress.	267
8.11	Contact between a disk and a block: (a) contact pressure at time 4 and (b) total load.	268
8.12	Contact between a disk and a block: total load for various penalty values.	268
8.13	Configurations for a frictional sliding: (a) initial configuration; (b) position at $t = 2$; (c) position at $t = 4$; (d) position at $t = 6$.	269
8.14	Resultant force history for sliding disk: (a) frictionless; (b) friction $\mu = 0.2$.	270
8.15	Initial and final configurations for a billet.	271
9.1	Shapes for pseudo-rigid and rigid body analysis: (a) ellipsoid; (b) faceted body.	278
9.2	Lagrange multiplier constraint between flexible and rigid bodies: (a) rigid-flexible body; (b) Lagrange multipliers.	283
9.3	Spinning disk constrained by a joint to a rigid arm.	286
9.4	Rigid-flexible model for spinning disk: (a) problem definition. Solutions at time (b) $t = 2.5$ units; (c) $t = 5.0$ units; (d) $t = 7.5$ units; (e) $t = 10.0$ units; (f) $t = 12.5$ units; (g) $t = 15.0$ units; (h) $t = 17.5$ units.	290

xxii List of Figures

9.5	Displacements for rigid-flexible model for spinning disk. Displacement at: (a) revolute; (b) disk rim.	291
9.6	Cantilever with tip mass: (a) $t = 2$ units; (b) $t = 4$ units; (c) $t = 6$ units; (d) $t = 10$ units; (e) $t = 12$ units; (f) $t = 14$ units; (g) $t = 16$ units; (h) $t = 18$ units; (i) $t = 20$ units.	292
9.7	Biofidelic rear impact dummy. Image courtesy of Dassault Systèmes SIMULIA.	292
9.8	Sorting of randomly sized particles. Image courtesy of Dassault Systèmes SIMULIA.	293
10.1	Open and closed balls in \mathbb{R}^n .	300
10.2	An open set along with its boundary and closure.	300
10.3	One-dimensional example of a tangent space to the graph of f at a point \mathbf{x}_0 .	304
10.4	The tangent space at a point of an open set.	304
10.5	The tangent map.	305
10.6	Intrinsic interpretation of the tangent map.	307
10.7	A body in \mathbb{R}^3 .	307
10.8	Coordinate parameterization of a body.	308
10.9	The tangent basis vectors.	311
10.10	A one-dimensional example of a tangent vector.	312
10.11	A simple body parameterized by the functions $\Phi : \Omega \rightarrow \mathbb{R}^3$ and $\phi : \Gamma \rightarrow \mathbb{R}^3$.	312
10.12	A simple surface in \mathbb{R}^3 .	317
10.13	The transition map $\varphi_2^{-1} \circ \varphi_1 : \Omega_1 \subset \mathbb{R}^2 \rightarrow \Omega_2 \subset \mathbb{R}^2$.	317
10.14	Coordinate lines on a simple surface.	319
10.15	A coordinate transformation function $f : \mathcal{V} \subset \mathbb{R}^2 \rightarrow \mathcal{U} \subset \mathbb{R}^2$.	320
10.16	Important notation for linear elasticity.	324
10.17	A parameterized body in \mathbb{R}^3 .	326
10.18	Notation for the reference parameterization of a shell.	332
10.19	The mid-surface basis vectors.	334
10.20	Through the thickness surfaces \mathcal{S}^α defined by holding the coordinate ξ^α constant.	335
10.21	The differential force acting on the surface \mathcal{S}^1 with tangent basis vectors and unit normal.	336
10.22	The differential element of moment about the mid-surface acting on the surface \mathcal{S}^1 .	337
10.23	Through the thickness sections \mathcal{S}^3 .	338
10.24	A finite rotation and stretch of the director \mathbf{d}^0 .	347
10.25	Reference geometry of the shell.	367
10.26	Complex shell with stiffener panels. A global parameterization of the type $\mathbf{x} = \varphi^0(\xi^1, \xi^2)$ is not possible.	367

10.27	A four-node quadratic element parameterization of the shell mid-surface S_e .	370
10.28	Notation for the assumed strain field on the standard isoparametric element.	382
10.29	Cylindrical bending of a flat strip.	385
10.30	(a) w : Vertical displacement; (b) θ_x : Rotation; (c) M_x : Bending moment for cylindrical bending of a flat strip: 20 element solution.	386
10.31	Barrel (cylindrical) vault: (a) barrel vault geometry and properties; (b) vertical displacement of center section; (c) longitudinal displacement of support. 16×24 element mesh.	387
10.32	Barrel vault of Fig. 10.31. (a) M_1 , transverse; M_2 , longitudinal; center-line moments. (b) M_{12} , twisting moment at support. 16×24 element mesh.	388
10.33	Barrel vault of Fig. 10.31. Contours of vertical displacement u_1 .	388
10.34	Spherical cap: (a) geometry; (b) 768-element mesh.	389
10.35	Spherical cap: (a) radial (u) and (b) vertical (w) displacements for 768-element mesh.	390
11.1	Illustration of the definition of a transition or overlap map on a differentiable manifold.	394
11.2	Two charts covering the unit circle $S^1 \subset \mathbb{R}^2$.	395
11.3	A manifold and a local coordinate chart.	396
11.4	Chart (\mathcal{U}, χ) on the unit circle.	397
11.5	North pole chart in the unit sphere.	398
11.6	Differentiability of a map.	398
11.7	Tangent space to a surface in \mathbb{R}^3 .	399
11.8	Manifold of diffeomorphisms on $\Omega \subset \mathbb{R}^n$.	401
11.9	Tangent map between two manifolds.	402
11.10	Two parameterizations of the same curve $\mathcal{C} \subset \mathbb{R}^3$.	404
11.11	Velocity vector as a tangent field.	406
11.12	Illustration of a vector field along \mathcal{C} .	406
11.13	A curve \mathcal{C} and a moving frame, given by mappings $(\varphi, \Lambda) : I \rightarrow \mathbb{R}^3 \times SO(3)$.	407
11.14	Covariant derivative on a hyper-surface.	423
11.15	Geometric interpretation of the exponential map.	425
11.16	Geodesics do not necessarily minimize distance.	428
11.17	Geometric interpretation of the exponential map in $GL(3, \mathbb{R})$.	434
11.18	Geometric interpretation of $\Lambda \in SO(3)$.	440
11.19	Geometric significance of $\exp[\hat{\Theta}]$: a rotation about $\Theta \in \mathbb{R}^3$ of magnitude $\ \Theta\ \in \mathbb{R}$.	442
12.1	Simple body model. A placement $S \subset \mathbb{R}^3$ of \mathcal{P} in a configuration $\kappa : \mathcal{P} \rightarrow S \subset \mathbb{R}^3$ is an open set $S = \kappa(\mathcal{P}) \subset \mathbb{R}^3$.	450

xxiv List of Figures

12.2	Classical setup of continuum mechanics. We think of $\mathcal{B} = \kappa_0(\mathcal{P})$ (the <i>reference</i> placement) and $\mathcal{S}_t = \kappa_t(\mathcal{P})$ (the <i>current</i> placement) as <i>manifolds</i> .	450
12.3	Geometric setup. Mappings between differentiable manifolds.	452
12.4	The convective coordinate system $\mathbf{X} = \chi_0(\xi^1, \xi^2, \xi^3)$ and $\mathbf{x} = \chi(\xi^1, \xi^2, \xi^3)$ for the same $\xi = (\xi^1, \xi^2, \xi^3) \in \Omega$.	452
12.5	Coordinate curves and base vectors of a chart (χ, Ω) .	455
12.6	The setup for stress tensors and traction vectors.	462
13.1	Basic geometric objects.	468
13.2	Two configurations of a rod in Euclidean space.	470
13.3	Interpretation of the strain measure γ_t .	476
13.4	A rod as a three-dimensional body occupying placements $\mathcal{S}_t \subset \mathbb{R}^3$.	479
13.5	Force element on a cross-sectional area \mathcal{A}_t .	481
13.6	Setup for balance laws.	494
13.7	$\chi_0 \equiv \text{identity}$, $D\chi_0 = \mathbf{1}$, $\Lambda_0 = \mathbf{1}$, $j_0 = 1$, $\mathbf{H}_0 \equiv \mathbf{0}$.	494
13.8	Parameterized by reference arc length, $\mathbf{t}_3^0 \equiv \frac{\partial \varphi_0}{\partial S}$.	498
13.9	Circular ring geometry and deformed shapes: (a) geometry; (b) deformed shapes.	512
13.10	Circular ring load-displacements.	512
13.11	Cantilever L-beam geometry: (a) cross-section A-A; (b) cross-section B-B.	513
13.12	Cantilever L-beam deformed shapes: (a) cross-section; (b) cross-section B-B.	514
13.13	Cantilever L-beam. Load-displacement at tip: (a) cross-section A-A; (b) cross-section B-B.	514
13.14	Co-linear loaded cantilever beam geometry.	514
13.15	Co-linear loaded cantilever beam. Deformed configuration at four time stages: (a) $t = 0.05$; (b) $t = 0.095$; (c) $t = 0.15$; (d) $t = 0.20$.	515
13.16	Co-linear loaded cantilever beam. Plot of tip displacement components vs. time.	515
14.1	The shell body.	521
14.2	A deformation of the shell.	522
14.3	A three-dimensional parameterization of the shell-like body.	525
14.4	Finite rotations in S^2 : the vector $\mathbf{t}_{x_0}^0$ is rotated to \mathbf{t}_x by the angle $\ \mathbf{t}_\Delta\ $, with axis of rotation along Θ . Here $\Theta := \mathbf{t}_{x_0}^0 \times \mathbf{t}_\Delta$.	555
14.5	A four-node quadrilateral element parameterization of the shell mid-surface \mathcal{S}_e .	563
14.6	Geometric interpretation of the update procedure for the director field. Each nodal director describes a curve on S^2 composed of <i>arcs of geodesic</i> (i.e., arcs of great circle).	567

14.7	Geometric update procedure in S^2 . Nodal directors, which are updated by means of the exponential map, rotate by the amount $\Delta\Lambda_a^k$.	568
14.8	Notation for the assumed strain field on the standard isoparametric element.	578
14.9	Shell model for L-beam: undeformed and deformed view.	582
14.10	Centerline load-displacement for L-beam. Comparison of shell and beam models. Solid lines: shell; dotted line: beam.	582
14.11	Pinched hemisphere: (a) problem geometry; (b) 4×4 mesh and forces.	583
14.12	Pinched hemisphere. Displacements at force locations: (a) displacement; (b) Pian-Sumihara.	584
14.13	Pinched hemisphere. Displacement contours on deformed configuration: (a) u_1 displacement; (b) u_2 displacement.	584
14.14	Buckling of skin-stringer panel. Image courtesy of Dassault Systemes SIMULIA.	585
14.15	Car crash simulation. Image courtesy of Livermore Software Technology Corporation.	585
A.1	Parent coordinates for a quadrilateral.	598
A.2	Node numbering for four-node and nine-node quadrilateral elements.	599
A.3	Parent coordinates and node order for an eight-node brick element.	600
A.4	Parent coordinates and node order for triangular elements: (a) three-node triangle and area coordinates; (b) six-node triangle.	602
A.5	Node order for linear and quadratic tetrahedron elements.	603

